RSC Advances

PAPER

Check for updates

A facile synthesis of molybdenum carbide nanoparticles-modified carbonized cotton textile as an anode material for high-performance microbial fuel cells†

Lizhen Zeng,[ac] Shaofei Zhao,[b] Lixia Zhang[d] and Miao He [iD] *[a]

A novel macroscale porous structure electrode, molybdenum carbide nanoparticles-modified carbonized cotton textile (Mo_2C/CCT), was synthesized by a facile two-step method and used as an anode material for high-performance microbial fuel cells (MFCs). The characterization results show that the carbonized cotton textile modified with Mo_2C nanoparticles offers a great specific surface area (832.17 m^2 g^{-1}) for bacterial adhesion. The MFC using Mo_2C/CCT anode delivers the maximum power density of 1.12 W m^{-2}, which is 51% and 116% higher than that of CCT and unmodified carbon felt anodes under the same conditions. The high power density is mainly due to the Mo_2C nanoparticles with good biocompatibility and high conductivity and superior electrochemical activity, as well as the macroscale porous structure of carbonized cotton textile, which facilitate the formation of electroactive biofilm and improve the electron transfer. This paper introduces a feasible way to synthesize cost-effective and high-performance anode materials for MFCs.

1 Introduction

As a representative bio-electrochemical system, microbial fuel cells (MFCs) can use microorganisms to decompose waste, achieving waste treatment and producing electricity with mild operating conditions and environmentally friendly characteristics, which has provided a new direction to solve energy and environmental issues and become a hot research topic in recent years.[1–3] However, the large-scale commercial applications of MFCs have been mainly inhibited by the low power density and high cost of MFCs.[4,5]

Unlike hydrogen fuel cells and other chemical fuel cells, due to the role of microorganisms, the anode is regarded as a crucial factor affecting the performance of MFCs, which exerts a great impact on bacterial adhesion, electron transfer and substrate oxidation.[6,7] Therefore, a suitable anode material is beneficial to improve the performance of MFCs. Accordingly, an ideal anode

material requires good biocompatibility, excellent conductivity, excellent stability, large specific surface area, high porosity and low-cost.[7,8] Nowadays, carbon-based materials and graphite-based materials are the most used commercial anode materials in MFCs, while their relatively smooth surfaces are not conducive to the bacterial adhesion.[9] If insufficient bacterial cells adhere on the anode, the transfer efficiency of electrons from the microbial metabolism to the anode *via* extracellular electron transport (EET) is hindered and hence limits the performance of MFCs.[3,10] Thus, the low performance of anode material is the major obstacle to limiting the power density of MFCs.[11]

In our previous report, CCT and NC@CCT have been developed as low-cost and high-performance anode materials of MFCs.[8] Yet, CCT and NC@CCT exhibits poor electrocatalytic activity. Noble metal nanomaterials have been explored as anode materials to improve the catalytic performance of MFCs.[3] In order to improve the electrochemical activity of CCT for facilitating the catalytic oxidation of substrate, modifying with noble metal (such as Pt) nanomaterials could be a good idea.[3] Pt nanoparticles are excellent electrocatalyst material, have superior performance, such as good catalytic activity and high electron transfer efficiency, which are very suitable for applicable in catalysts and other fields.[3,12] However, the high cost of Pt-based materials has limited their application.[13] As we all know, molybdenum carbide (Mo_2C) is one of classic transition metal carbides, which not only has Pt-like electronic and catalytic properties, but also low-cost.[14–17] Mo_2C nanomaterials

[a]*School of Physics and Optoelectronic Engineering, Guangdong University of Technology, Guangzhou 510006, China. E-mail: herofategdut@126.com*

[b]*School of Chemical Engineering and Light Industry, Guangdong University of Technology, Guangzhou 510006, China*

[c]*Analysis and Testing Center, South China Normal University, Guangzhou 510006, China*

[d]*CAS Key Laboratory of Environmental and Applied Microbiology, Environmental Microbiology Key Laboratory of Sichuan Province, Chengdu Institute of Biology, Chinese Academy of Sciences, Chengdu 610041, China*

possess high electrical conductivity and unique catalytic activity for many chemical processes, such as fast redox reactions with protons on the surface.[18] More importantly, Mo_2C nanoparticles exhibit good biocompatibility and excellent electrocatalytic activity towards oxidation of bacterial metabolites.[19–22] Unfortunately, as previously reported, the conditions for synthesis of Mo_2C nanoparticles are very strict and the true of product is hard to control.[20,21]

In this study, Mo_2C/CCT was developed as anode material for high-performance MFCs *via* a facile two-step method (dipping and carbonization treatment). The Mo_2C/CCT electrode provides a high conductivity, a rough surface and a large specific surface area for bacterial adhesion on the anode, facilitates the formation of electroactive biofilm, as well as displays superior electrochemical activity. The MFC using Mo_2C/CCT anode has better performance than which using CCT and unmodified carbon felt anodes under the same conditions. This paper demonstrates a feasible method to prepare cost-effective and high-performance anode material for MFCs.

2 Materials and methods

2.1 Preparation of Mo_2C/CCT

Mo_2C/CCT was prepared *via* a facile two-step method (dipping and carbonization method). Typically, waste cotton textiles were prepared according to our previous report.[8] As-prepared cotton textile was dipped into 2 mol L^{-1} ammonium heptamolybdate tetrahydrate (($NH_4)_6Mo_7O_{24}\cdot4H_2O$, Aladdin) aqueous solution under stirring for 24 h, then dried at 60 °C for 24 h. Finally, the dried ammonium molybdate modified cotton textile (AM/CCT) was carbonized at 1000 °C for 1 h under inert gas (Ar) condition. The blank CCT was used for comparison. In addition, using the same method, cotton textiles dipped in different concentrations of $(NH_4)_6Mo_7O_{24}\cdot4H_2O$ aqueous solution (1 mol L^{-1} and 3 mol L^{-1}) and carbonized, which were denoted as Mo_2C/CCT-1 and Mo_2C/CCT-3, respectively.

2.2 Materials characterization

The XRD patterns of Mo_2C/CCT and CCT were recorded on Bruker D8 Advance X-ray diffractometer (Germany) with Cu Kα radiation (λ = 1.5405 nm). The Raman spectroscopy was recorded with a confocal microscope Raman spectrometer system (Lab RAM Aramis, HORIBA, France). The surface morphologies of samples and biofilms were characterized with field emission-scanning electron microscopy (FE-SEM, ZESISS Gemini 500, Germany). The samples and biofilms were coated with platinum (Pt) with a coating device (Quorum Q150TES, UK) before observation. The energy dispersive X-ray microanalysis system (EDS) analysis and the quantitative element mapping analysis were carried out on Oxford instrument IET250 spectrometer (Oxford, UK). The X-ray photoelectron spectroscopy (XPS) measurements were measured using ESCALAB 250 (Thermo Fisher Scientific, USA) with an Al Kα (mono) irradiation (1486.6 eV). The electrical resistivity measurement was carried out on a four-probe conductivity measurement device (RST-8, Guangzhou). The specific surface area of Mo_2C/CCT and CCT samples were measured using an accelerated surface area and porosimetry system (Micrometrics, ASAP 2020, USA) and calculated according to Brunauer–Emmett–Teller (BET) method.

2.3 MFC construction, operation and tests

Universal air-cathode cylindrical MFCs were constructed as Logan *et al.* previously reported.[23] The Mo_2C/CCT anode (2.0 cm × 2.0 cm × 0.1 cm) and cathode were connected to an external resistor (1000 Ω) *via* titanium wire. CCT and unmodified carbon felt (CF) electrodes with the same size were also used as anodes for comparison. The cathode was a carbon paper coated with Pt/C catalyst (0.5 mg cm^{-2} Pt loading) and prepared as described in previous report.[24]

The MFC reactors were inoculated with 5.0 mL mixed bacterial suspension from the effluent of matured single-chamber MFC which had been originally inoculated with activated anaerobic sludge.[24] The reactors were fed with sodium acetate-growth medium including sodium acetate (1 g L^{-1}) as the electron donor and culture medium solution consisting of 50 mmol phosphate buffer solution (pH 7.0), 12.5 mL L^{-1} vitamin solution and 12.5 mL L^{-1} mineral solution. When the MFCs approached steady state, the polarization and power density curves were obtained by changing the external resistance from 8000 to 100 Ω. The power density (P, W m^{-2}) was calculated as follows: $P = U^2/R$, where U (V) and R (Ω) are the output voltage and the external resistance, respectively. The P was normalized by the projected area of anode surface (4.0 cm^2). The MFCs were operated in batch-fed mode at 30 °C. All the measurements were performed with three MFCs for each sample.

Electrochemical measurements were performed on an electrochemical station (Autolab PGSTAT-302N, Metrohm Co., Switzerland) with a traditional three-electrode system: the anode, the saturated calomel electrode (SCE) and the titanium wire were used as the working electrode, reference electrode and counter electrode, respectively. The chronopotentiometry (CP) was measured after the MFC forming a stable biofilm with the applied current of 0.1 μA. The electrochemical impedance spectroscopy (EIS) was conducted at open circuit potential *versus* SCE in a frequency range from 10 000 to 0.01 Hz with an amplitude of 5 mV.

3 Results and discussion

3.1 Characteristics of Mo_2C/CCT

The Mo_2C/CCT was synthesized by a facile two-step method. Fig. 1 illustrates the synthesis procedure of Mo_2C/CCT. The techniques of XRD and Raman spectroscopy were utilized to determine the composition of the prepared sample. Fig. 2a presents the XRD patterns of Mo_2C/CCT and CCT. As shown in Fig. 1a, the Mo_2C/CCT has several main diffraction peaks at 26.7°, 37.9°, 61.1°, 67.5° and 79.7°, which was corresponding with Mo_2C (JCPDS, no. 35-787). The diffraction peak was at 26.7°, which can be assigned as the (002) reflection of graphite, corresponding to a graphitic carbon. No other peak could be
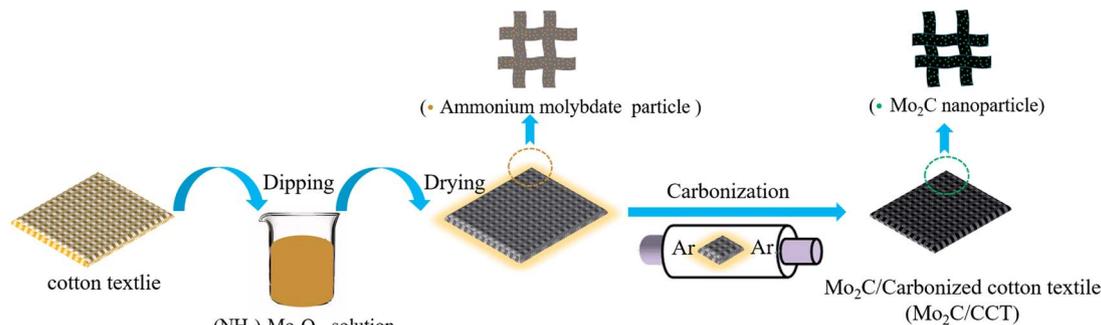
Fig. 1 Schematic illustrating the synthesis route of Mo$_2$C/CCT.

detected. Comparing with the X-ray diffraction pattern of CCT, it can be concluded that the Mo$_2$C/CCT mainly contains Mo$_2$C. Fig. 2b presents the Raman spectrum of the Mo$_2$C/CCT and CCT, there are two characteristic peaks around 1350 and 1600 cm^{-1} corresponding to the D and G bands of graphitic carbon. Notably, the Raman spectrum of Mo$_2$C/CCT contains a weak peak around 970 cm^{-1}, which can be attributed to the characteristic band of molybdenum carbide.[25–27] The results of XRD and Raman spectroscopy demonstrate that the prepared sample has been successfully modified with Mo$_2$C nanoparticles.

The energy dispersive X-ray microanalysis system (EDS) analysis was further used to confirm the composition of Mo$_2$C/CCT and CCT. As Fig. 2c depicted, the Mo$_2$C/CCT is mainly

composed of C, O, Mo and trace Si elements. Pt originates from the EDS measurement. While as, only C, O and trace Si elements can be detected in CCT. Consequently, the Mo$_2$C/CCT sample contains Mo$_2$C. It is worth noting that all elements don't have effect on the growth of bacteria in the MFC experiments. Fig. 2d shows the nitrogen adsorption–desorption isotherm curves of Mo$_2$C/CCT and CCT, both of which represent typical IV characteristics, and the corresponding specific surface area of Mo$_2$C/CCT composite is about 832.17 m^2 g^{-1}, which is about four times higher than that of CCT (209.64 m^2 g^{-1}). Therefore, it illustrates that the Mo$_2$C/CCT provides a larger specific surface area and more potential active sites for bacterial adhesion and growth.[28]
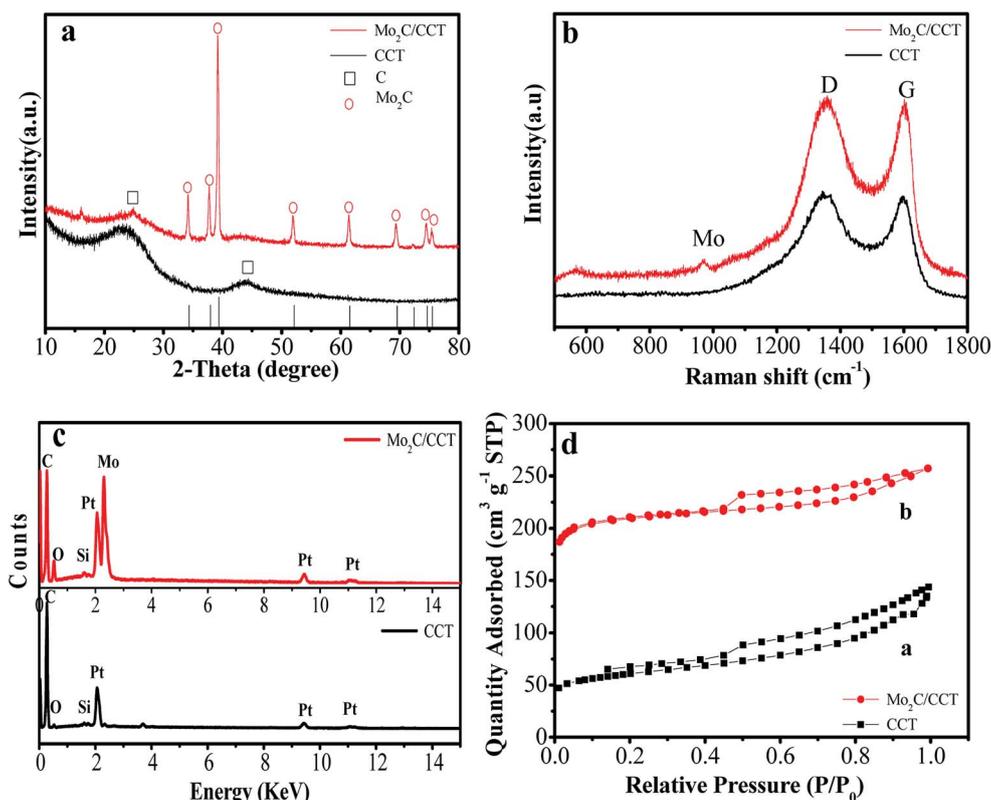

Fig. 2 X-ray diffraction patterns (a); Raman spectra (b); energy-dispersive X-ray spectra (c); nitrogen adsorption–desorption isotherms (d) of Mo$_2$C/CCT and CCT samples.
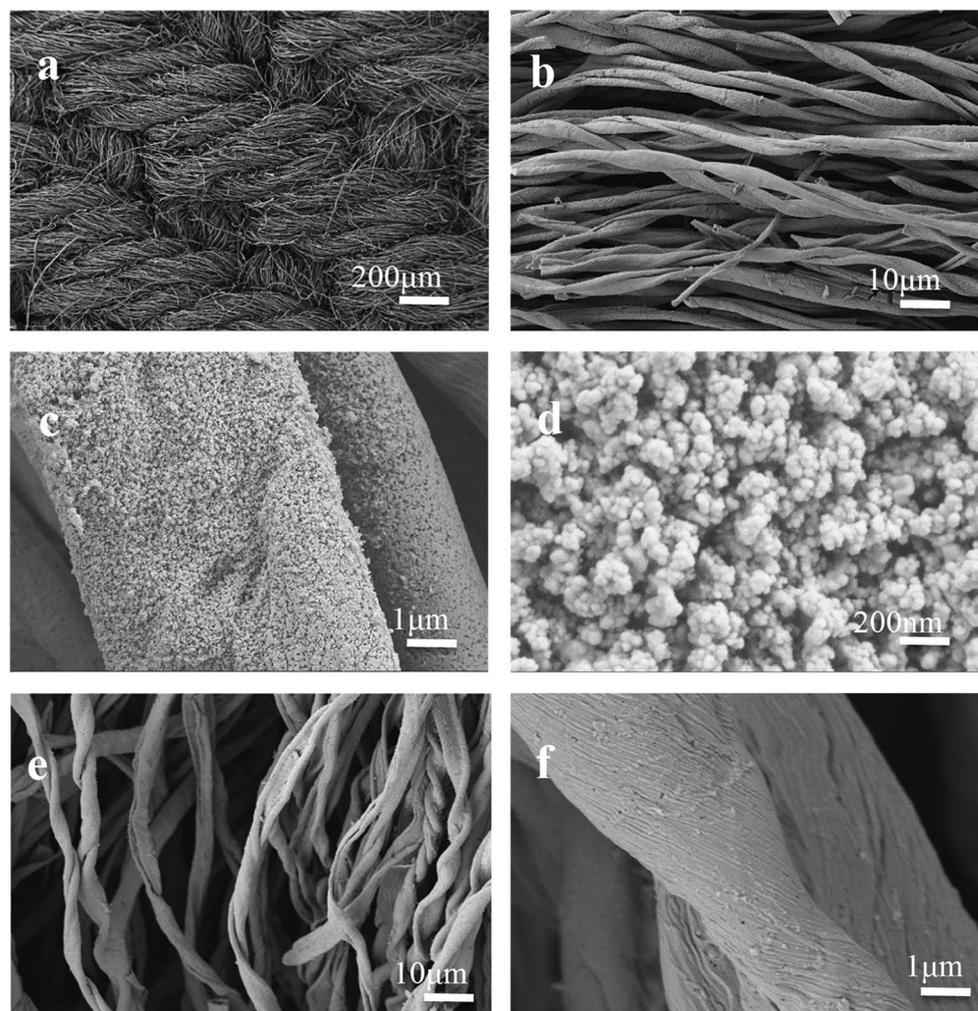
Fig. 3 SEM images of Mo$_2$C/CCT (a–d) and CCT (e and f) at various magnifications.

The morphology of Mo$_2$C/CCT was characterized by FESEM. Fig. 3 shows the SEM images of Mo$_2$C/CCT and CCT at various magnifications. It can be observed easily from Fig. 3a and b that, the Mo$_2$C/CCT is composed of fibers. The macroscale porous structure of the intertwined carbonized cotton textile fibers (Fig. 3b) produces an open space (approximately 10 μm). As Fig. 3c depicted, the fiber is coated by many nanoparticles after simple dipping of ammonium molybdate and carbonization treatment. Obviously, it is seen from the high-resolution SEM image of Mo$_2$C/CCT (Fig. 3d) that many nanoparticles are modified on the fiber surface and the surface of Mo$_2$C/CCT is highly rough. Notably, the surface of CCT was relatively smooth (Fig. 3e and f). The good conductivity and rough surface of Mo$_2$C nanoparticles could result in stronger electrostatic interaction and faster electron transfer rate between bacteria and anode, thus largely increases the loading amount of bacteria.[22]

To reveal the surface compositions and electronic state of Mo$_2$C/CCT, X-ray photoelectron spectroscopy (XPS) measurement was carried out. As depicted in the survey XPS spectrum (Fig. 4a), five characteristic signals locate at 233.6, 285.8, 398.1, 416.5, 532.2 eV, corresponding to Mo 3d, C 1s, N 1s, Mo 3p and

O 1s, respectively.[29] From the C 1s spectra of Mo$_2$C/CCT (Fig. 4b), the characteristic peaks at 284.4, 284.8 and 285.5 eV can be attributed to C–Mo, C=C and C–C, respectively.[29,30] The Mo 3d spectra of Mo$_2$C/CCT (Fig. 4c) shows the diffraction peaks at 232.0, 232.8, 234.5, 235.6, 236.2 eV, which can be attributed to Mo 3d of Mo$_2$C and oxidized molybdenum with intermediate oxidation states (MoO$_x$). The MoO$_x$ may be generated by the oxidization of Mo$_2$C during the XPS measurement. From the N 1s spectra (Fig. 4d), the characteristic peaks at 397.6, 398.4, 399.8 and 401.7 eV, which are assigned to pyridinic, pyrrolic, graphitic and oxidized nitrogen, respectively.[31] The nitrogen group might be coated on the Mo$_2$C/CCT sample due to pyrolysis of ammonium molybdate. As Tang *et al.* reported, nitrogen-doped on the anode will enhance biocatalytic activity and thus favors bacterial adhesion and facilitates electron transfer between anode and bacteria.[32] Besides, carbon-based anodes have been treated with ammonia to strengthen the interaction between the anode and the bacteria.[33]

In order to further determine the element composition and distribution of Mo$_2$C/CCT, the corresponding EDS quantitative element mapping analysis was performed. The SEM image of
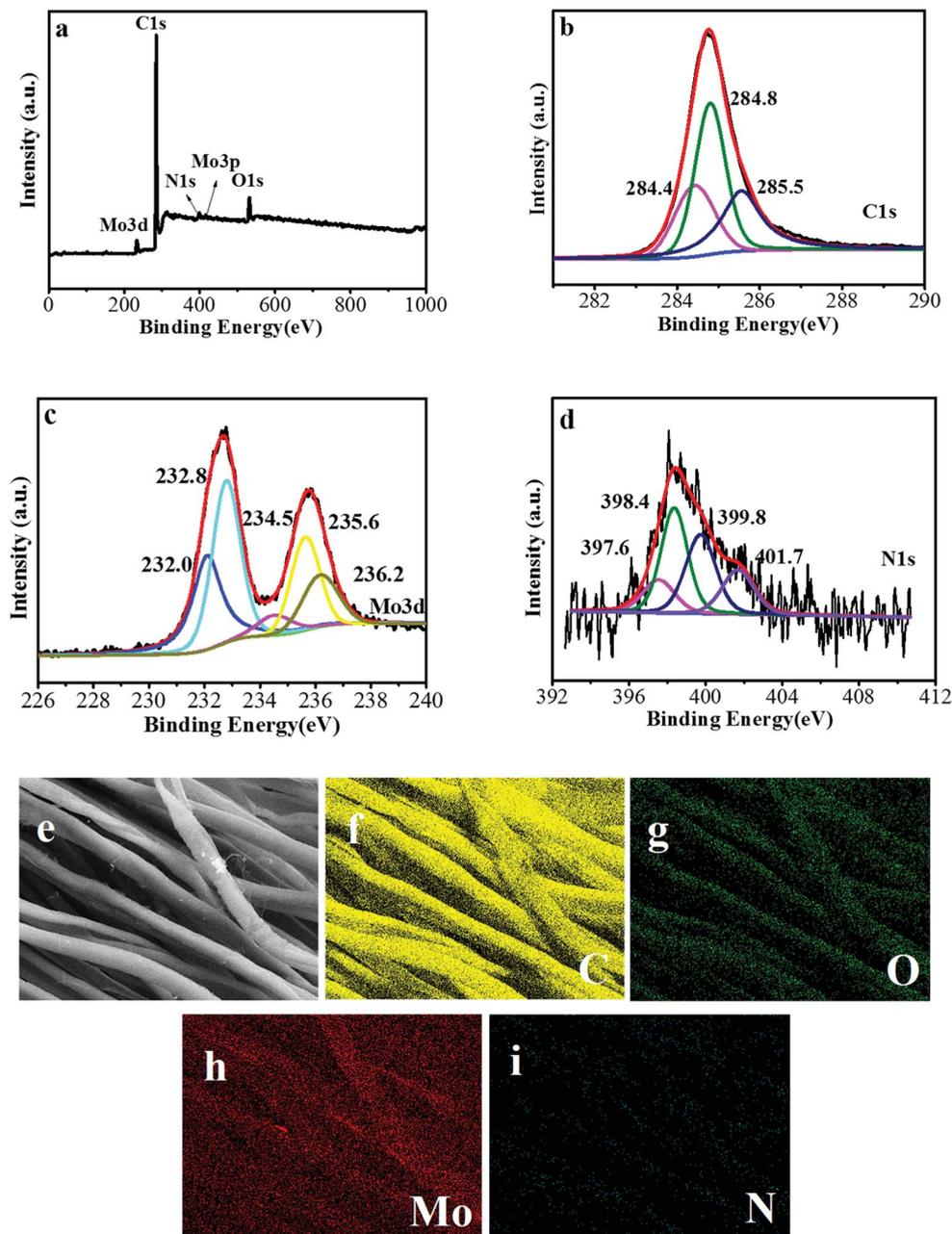
Fig. 4   X-ray photoelectron spectroscopy (XPS) survey of Mo₂C/CCT (a); high-resolution C 1s (b), Mo 3d (c) and N 1s (d) XPS scans of Mo₂C/CCT sample; and the SEM image of Mo₂C/CCT (e) and the corresponding quantitative EDS element mapping of C (f), O (g), Mo (h), and N (i).

Mo$_2$C/CCT and quantitative element mapping of C, O, Mo, and N are presented in Fig. 4e–i. As obviously seen from Fig. 4e–i, the C, O, Mo and N elements are evenly distributed on the surface of textile fibers, the content of N is the smallest, which is consistent with the XPS results.

3.2   Performance of MFCs

Compared with the blank CCT and unmodified carbon felt electrodes, the Mo$_2$C/CCT electrode was used as the anode for MFC. The batch-fed MFC was inoculated with mixed bacterial suspension from the effluent of matured single-chamber MFC, and then operated using sodium acetate as sole anodic electron donor (1 g L^{-1}). As depicted in Fig. 5a, when the voltage output drops around 0 V, 80% of anolyte of each MFC is replaced with the fresh anolyte. Subsequently, the current density quickly increases to the highest value, and then gradually declines due to the depletion of anolyte. After five cycles of operation, the relatively stable cell voltages for MFCs equipped with Mo$_2$C/CCT and CCT anodes are obtained. However, the MFC equipped with unmodified carbon felt (Fig. S1a†) anode just started up successfully after 200 h. It is also observed that the Mo$_2$C/CCT anode delivers the larger cell voltage than the CCT and the unmodified carbon felt (Fig. S1a†) anodes.
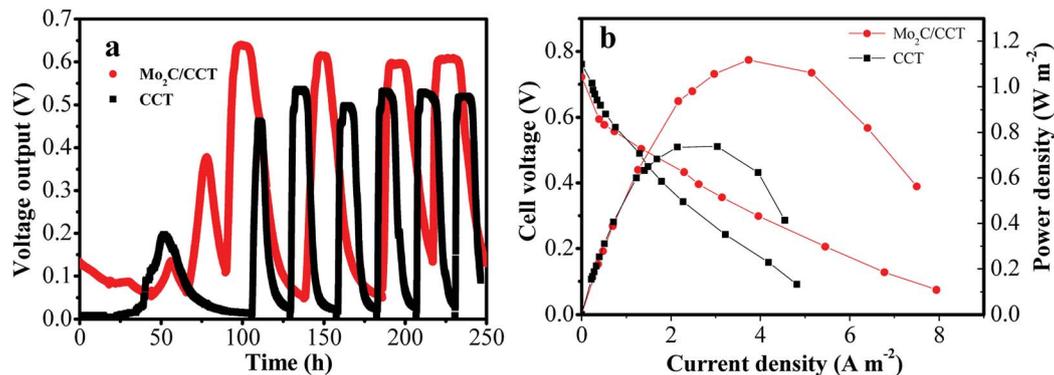
Fig. 5 Voltage output *versus* time during start-up of the MFCs with different anodes with 1000 Ω resistance loading (a); polarization curves and power outputs of different anodes in the MFCs (b).

The power production and polarization behavior of MFC were investigated after stable operation for three weeks of MFCs (Fig. 5b). It can be implied from Fig. 5a that the anode material has little influence on the open circuit voltage, but has an important effect on the power density. As illustrated in Fig. 5b and S1b,† the MFC equipped with Mo_2C/CCT anode delivers the maximum power density (1.12 W m^{-2}), which is 51% and 116% higher than that of CCT and unmodified carbon felt anodes, respectively. Table S1† shows a comparison of the performance of MFCs with different anode materials under the same type of single-chamber MFC and inoculum. It could be concluded that the anode performance can be greatly improved due to the modification of Mo_2C nanoparticles on the surface of CCT.

What's more, the power density of MFCs is related with the amount of Mo_2C nanoparticles on the surface of carbonized cotton textile, which can be seen from Fig. S3.† The power densities of MFCs equipped with Mo_2C/CCT-1 and Mo_2C/CCT-3 anode are 0.80 W m^{-2} and 0.92 W m^{-2}, respectively, which are less than that of Mo_2C/CCT. The different concentration of precursor solution leads to the inconsistency of the growth of Mo_2C nanoparticles on the CCT surface. Because of the low concentration of precursor solution, the amount of Mo_2C nanoparticles on the surface of the carbonized cotton textile is small and the distribution of Mo_2C nanoparticles may be not uniform. While, an excess of concentration of precursor solution, the Mo_2C nanoparticles coating may fall off. Therefore, the concentration of the precursor solution of 2 mol L^{-1} is more suitable.

3.3 Electrochemical activity

To confirm the anodic performance, the potential responses were measured from Mo_2C/CCT and CCT anodes in half-batch experiments with an applied current of 0.1 μA, reflecting the polarization of the anodes. As described in our previous reports, the more negative the electrode potential, the better the anode activity.[7,8] As presented in Fig. 6a, the electrode potential of Mo_2C/CCT is more negative than that of CCT, indicating that the Mo_2C/CCT electrode possesses superior electrochemical activity, owing to the Mo_2C nanoparticles coating. Besides, it

can be found that the Mo_2C/CCT electrode is very stable after constant-current discharge experiment for 20 h.

EIS measurement was carried out on the MFCs after inoculation to investigate the effect of Mo_2C/CCT on the electron transfer efficiency from bacteria to the anode. Fig. 6b presents the electrochemical impedance spectra of the Mo_2C/CCT and CCT electrodes. The R_{ohm} is ascribed to the ionic conductivity of the solution and the electronic conductivity of the electrode materials.[34,35] As Fig. 6b shown, R_{ohm} of Mo_2C/CCT is smaller than that of CCT electrode, owing to the high conductivity of Mo_2C nanoparticles. What is more, the electrical resistivity of Mo_2C/CCT (2.69 Ω sq^{-1}) is smaller than that of CCT (7.56 Ω sq^{-1}), which was recorded on a four-probe conductivity measurement device. Thus, the Mo_2C/CCT electrode has higher conductivity than CCT electrode. R_{ct} is the charge transfer resistance, which suggests the mechanism of electron transfer between the bacteria and the anode.[34] It is worth noting that the R_{ct} of Mo_2C/CCT electrode (11 Ω) is smaller than that of CCT electrode (57 Ω). The result suggests that the Mo_2C significantly reduces the electron transfer resistance but enhances the charge transfer rate between bacteria and anode.[36]

3.4 Biofilm of Mo_2C/CCT

The biocompatibility of the anode is mainly reflected in the easiness of biofilm formation on its surface.[22] The morphology of the biofilms on the Mo_2C/CCT and CCT electrodes were characterized by SEM after two months of steady operation. As displayed in Fig. 7a and b, the entire surface of the electrode is covered with rod-shaped bacterial cells. With the good biocompatibility of Mo_2C/CCT, the electrode fiber is wrapped by bacterial cells (Fig. 7c). It can be seen from the high-resolution SEM image (Fig. 7d) that bacterial cells are connected with each other by microbial nanowires (shown by the arrows) and the Mo_2C/CCT electrode isn't blocked by the bacterial cells after two months of operation. As a result, stable operation of the MFCs using Mo_2C/CCT anode is realized. However, a small amount of bacteria adhered on the CCT electrode can be found (Fig. 7e and f) and just a few bacterial cells are observed on the carbon felt electrode (Fig. S3†), which indicated that the modification of
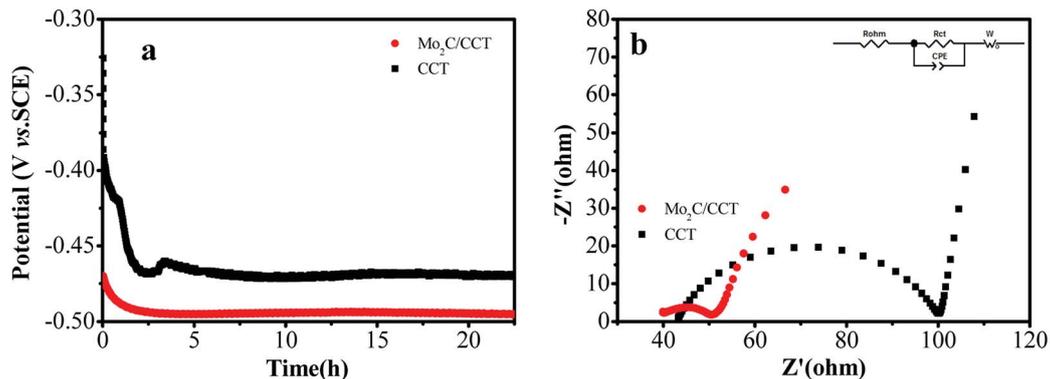
Fig. 6 Potential−time curves of different electrodes under a constant current of 0.1 μA (a); electrochemical impedance spectra of the electrodes (b) (inset: the equivalent circuit).

Mo_2C nanoparticles on the surface of CCT is beneficial to enhance the bacterial adhesion, further facilitates the formation of electroactive biofilm on the electrode.

With the above results, the electron-transfer mechanism at Mo_2C/CCT electrode was concluded as shown in Fig. S4.† The

electrons from the microbial metabolism are directly transferred to the Mo_2C/CCT electrode via direct contact or nanowires. Due to good biocompatibility of Mo_2C nanoparticles, bacterial cells are firmly attached to the surface of fiber through the electrostatic interaction between bacteria with rough
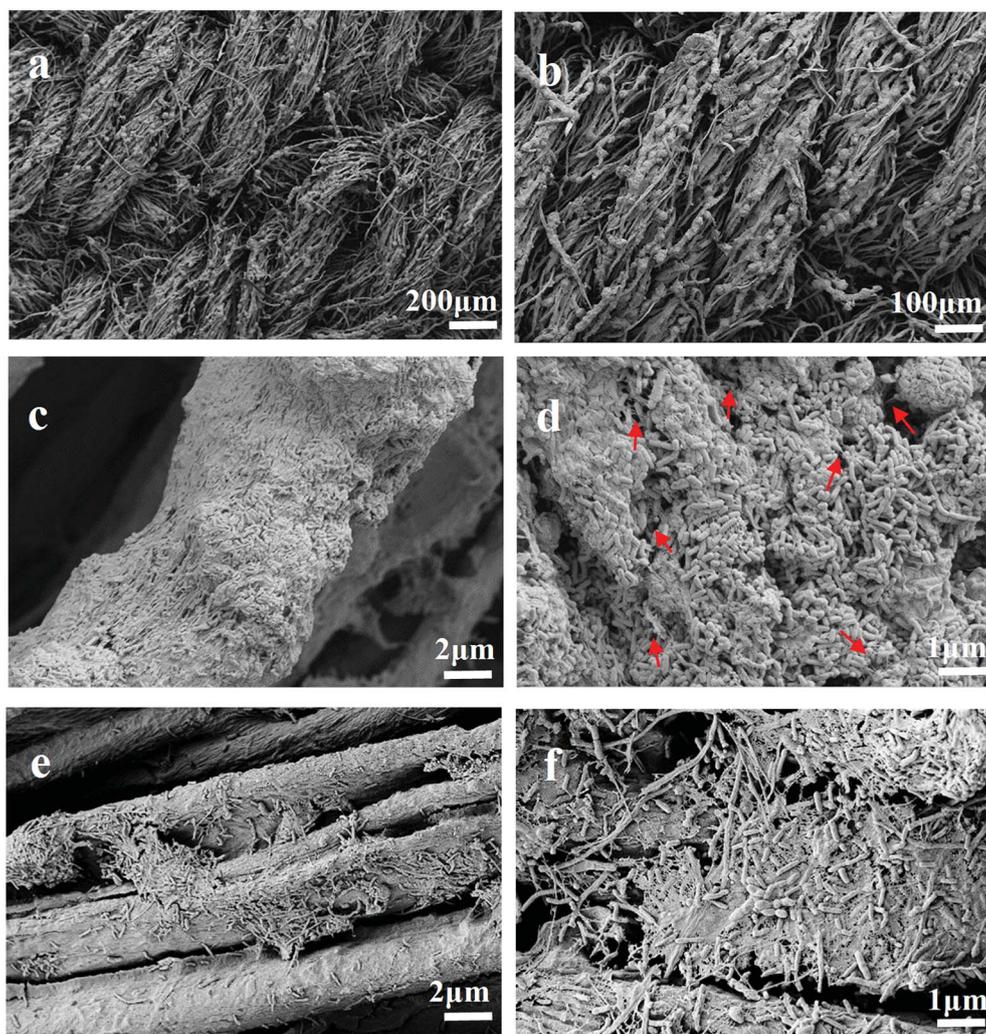

Fig. 7 SEM images of the electroactive biofilm grown on the Mo_2C/CCT (a−d) and CCT (e and f) anodes after two months of operation at various magnifications.

surface of Mo$_2$C nanoparticles (Fig. S4†), which facilitates the formation of electroactive biofilm. Moreover, Mo$_2$C nanoparticles possess the superior conductivity and electrochemical activity, which can accelerate the metabolically generated electrons transfer to the textile fiber (electrode).

4 Conclusions

In summary, we have successfully prepared the Mo$_2$C/CCT as an anode material for high-performance MFCs *via* a facile two-step method (dipping and carbonization treatment). The results show that the Mo$_2$C/CCT electrode offers a rough surface and a great specific surface area for bacterial adhesion on the anode, hence facilitates the formation of electroactive biofilm, as well as displays superior electrochemical activity and enhances the charge transfer rate between bacteria and electrode. The MFC using Mo$_2$C/CCT anode has better performance than which using CCT and unmodified carbon felt anodes. This paper demonstrates a feasible way to prepare cost-effective and high-performance anode material for MFCs.

Conflicts of interest

There is no conflict of interest to declare.

Acknowledgements

References

1 Y. Zhao, Y. Ma, T. Li, Z. Dong and Y. Wang, *RSC Adv.*, 2018, **8**, 2059–2064.

2 S. Chang, B. Huang, T. Wan, J. Chen and B. Chen, *RSC Adv.*, 2017, **7**, 56433–56439.

3 S. Kalathil and D. Pant, *RSC Adv.*, 2016, **6**, 30582–90592.

4 S. Chen, J. Tang, X. Jing, Y. Liu, Y. Yuan and S. Zhou, *Electrochim. Acta*, 2016, **212**, 883–889.

5 L. Yang, W. Deng, Y. Zhang, Y. Tan, M. Ma and Q. Xie, *Biosens. Bioelectron.*, 2017, **91**, 644–649.

6 Y. Yuan, T. Liu, P. Fu, J. Tang and S. Zhou, *J. Mater. Chem. A*, 2015, **3**, 8475–8482.

7 L. Zeng, W. Zhang, P. Xia, W. Tu, C. Ye and M. He, *Biosens. Bioelectron.*, 2018, **102**, 351–356.

8 L. Zeng, S. Zhao and M. He, *J. Power Sources*, 2018, **376**, 33–40.

9 B. E. Logan, *Appl. Microbiol. Biotechnol.*, 2010, **85**, 1665–1671.

10 Y. Fan, E. Sharbrough and H. Liu, *Environ. Sci. Technol.*, 2008, **42**, 8101–8107.

11 Y. C. Yong, X. C. Dong, M. B. Chan-Park, H. Song and P. Chen, *ACS Nano*, 2012, **6**, 2394–2400.

12 D. Chen, X. Zhuang, J. Zhai, Y. Zheng, H. Lu and L. Chen, *Sens. Actuators, B*, 2018, **255**, 1500–1506.

13 X. Zhuang, C. Tian, F. Luan, X. Wu and L. Chen, *RSC Adv.*, 2016, **6**, 92541–92546.

14 H. B. Wu, B. Y. Xia, L. Yu, X. Y. Yu and X. W. Lou, *Nat. Commun.*, 2015, **6**, 6512.

15 Y. Zhao, K. Kamiya, K. Hashimoto and S. Nakanishi, *J. Am. Chem. Soc.*, 2015, **137**, 110–113.

16 F. X. Ma, H. B. Wu, B. Y. Xia, C. Y. Xu and X. W. Lou, *Angew. Chem., Int. Ed.*, 2015, **54**, 15395–15399.

17 L. Liao, S. Wang, J. Xiao, X. Bian, Y. Zhang, M. D. Scanlon, X. Hu, Y. Tang, B. Liu and H. H. Girault, *Energy Environ. Sci.*, 2014, **7**, 387–392.

18 Q. Bkour, C. M. Cuba-Torres, O. G. Marin-Flores, S. Tripathi, N. Ravishankar, M. G. Norton and S. Ha, *J. Mater. Sci.*, 2018, **53**, 12816–12827.

19 W. Dai, H. Dong and X. Zhang, *Materials*, 2018, **11**, 1776–1786.

20 L. Zeng, L. Zhang, W. Li, S. Zhao, J. Lei and Z. Zhou, *Biosens. Bioelectron.*, 2010, **25**, 2696–2700.

21 L. Zeng, S. Zhao and W. Li, *Appl. Biochem. Biotechnol.*, 2015, **175**, 2637–2646.

22 Y. Wang, B. Li, D. Cui, X. Xiang and W. Li, *Biosens. Bioelectron.*, 2014, **51**, 349–355.

23 B. Logan, S. Cheng, V. Watson and G. Estadt, *Environ. Sci. Technol.*, 2007, **41**, 3341–3346.

24 Y. Yuan, S. G. Zhou, Y. Liu and J. H. Tang, *Environ. Sci. Technol.*, 2013, **47**, 14525–14532.

25 T. C. Xiao, A. P. E. York, H. Al-Megren, C. V. Williams, H. T. Wang and M. L. H. Green, *J. Catal.*, 2001, **202**, 100–109.

26 L. Pan, Y. Li, S. Yang, P. Liu, M. Yu and H. Yang, *Chem. Commun.*, 2014, **50**, 13135–13137.

27 J. Qiu, Z. Yang, Q. Li, Y. Li, X. Wu, C. Qi and Q. Qiao, *J. Mater. Chem. A*, 2016, **4**, 13296–13306.

28 L. Zhou, L. Sun, P. Fu, C. Yang and Y. Yuan, *J. Mater. Chem. A*, 2017, **5**, 14741–14747.

29 H. Li, H. Ye, Z. Xu, C. Wang, J. Yin and H. Zhu, *Phys. Chem. Chem. Phys.*, 2017, **19**, 2908–2914.

30 Y. Zhu, S. Wang, Y. Zhong, R. Cai, L. Li and Z. Shao, *J. Power Sources*, 2016, **307**, 552–560.

31 Q. Gao, X. Zhao, Y. Xiao, D. Zhao and M. Cao, *Nanoscale*, 2014, **6**, 6151–6157.

32 J. Tang, S. Chen, Y. Yuan, X. Cai and S. Zhou, *Biosens. Bioelectron.*, 2015, **71**, 387–395.

33 Y. J. Feng, Q. Yang, X. Wang and B. E. Logan, *J. Power Sources*, 2010, **195**, 1841–1844.

34 H. Li, B. Liao, J. Xiong, X. Zhou, H. Zhi, X. Liu, X. Li and W. Li, *J. Power Sources*, 2018, **379**, 115–122.

35 L. Zeng, X. Chen, H. Li, J. Xiong, M. Hu, X. Li and W. Li, *Electrochim. Acta*, 2018, **283**, 528–537.

36 C. Zhang, P. Liang, X. Yang, Y. Jiang, Y. Bian, C. Chen, X. Zhang and X. Huang, *Biosens. Bioelectron.*, 2016, **81**, 32–38.